

Article

# Boron Trifluoride Anionic Side Groups in Polyphosphazene Based Polymer Electrolyte with Enhanced Interfacial Stability in Lithium Batteries

Sebastian Schmohl <sup>†</sup>, Xuan He <sup>†,\*</sup>  and Hans-Dieter Wiemhöfer 

Institute of Inorganic and Analytical Chemistry, University of Münster, Corrensstraße 28/30, 48149 Münster, Germany; sebastian.schmohl@uni-muenster.de (S.S.); hdw@uni-muenster.de (H.-D.W.)

\* Correspondence: x\_he0002@uni-muenster.de; Tel.: +49-251-83-33113

<sup>†</sup> These authors contributed equally to this work

Received: 10 November 2018; Accepted: 3 December 2018; Published: 5 December 2018



**Abstract:** A modified polyphosphazene was synthesized using a mixed substitution at phosphorus consisting of 2-(2-methoxyethoxy)ethoxy side groups and anionic trifluoroborate groups. The primary goal was to increase the low lithium ion conductivities of the conventional lithium salt containing poly[2-(2-methoxyethoxy)ethoxy-phosphazene] (MEEP) by the immobilized anionic groups. As in previous studies, the mechanical stability was stabilized by UV induced radiation cross linking. By variation of the molar ratio between different side groups, mechanical and electrochemical properties are controllable. The polymer demonstrated large electrochemical stability windows ranging between 0 and 4.5 V versus the Li/Li<sup>+</sup> reference. Total and lithium conductivities of  $3.6 \times 10^{-4} \text{ S}\cdot\text{cm}^{-1}$  and  $1.8 \times 10^{-5} \text{ S}\cdot\text{cm}^{-1}$  at 60 °C were revealed for the modified MEEP. When observed in special visualization cells, dendrite formation onset time and short-circuit time were determined as 21 h and 90 h, respectively, under constant current polarization (16 h and 65 h for MEEP, both with 15 wt % LiBOB), which hints to a more stable Li/polymer interface compared to normal MEEP. The enhanced dendrite suppression ability can be explained by the formation of a more conductive solid electrolyte interphase (SEI) and the existence of F-contained SEI components (such as LiF). With the addition of ethylene carbonate–dimethyl carbonate (EC/DMC) to form MEE-co-OB<sub>3</sub>P gel polymer, both total and lithium conductivity were enhanced remarkably, and the lithium transference numbers reached reasonable values ( $\sigma_{\text{total}} = 1.05 \text{ mS}\cdot\text{cm}^{-1}$ ,  $\sigma_{\text{Li}^+} = 0.22 \text{ mS}\cdot\text{cm}^{-1}$ ,  $t_{\text{Li}^+} = 0.18$  at 60 °C).

**Keywords:** Polyphosphazene; polymer electrolyte; electrochemical stability; lithium metal battery

## 1. Introduction

Polymer electrolytes (SPEs) offer improved safety and reliability as compared to electrolytes based on liquid solvents only [1–7]. An additional advantage might be an enhanced stability towards lithium dendrite formation in contact with lithium metal anodes as was reported by several authors [8–12]. However, the achievable steady-state lithium ion current densities suffer from the very low lithium ion conductivities as well as the low transference numbers,  $T_+$ , which typically range between 0.1 and 0.25 [13–15].

Therefore, polymer electrolytes are usually transformed to polymer gels by gelification with polar aprotic liquids, which largely enhance the ionic mobility [16–19]. An additional improvement is expected by the use of polymers with immobilized anions (= polyanions) whose charge is compensated by mobile lithium ions. This strategy should lead to single lithium ion transport and a transference number equal to one. There have been several studies reporting experiences on

this concept regarding different polymers [20–25]. Allcock et al. was already able to synthesize a polyphosphazene based single ion conductor with arylsulfonimide side groups covalently linked to the polymer backbone. The lithium ion concentration depended on the net percentage of lithiated sulfonamide substituents, but as most often found by these and other authors before, the mobility of ions remained small, reaching  $2.45 \times 10^{-6} \text{ S cm}^{-1}$  at ambient temperatures and  $4.99 \times 10^{-5} \text{ S cm}^{-1}$  at  $80 \text{ }^\circ\text{C}$  [26]. Such values do not yet meet the requirements of practical batteries. Fiedler et al. synthesized the polyphosphazene based polymer electrolytes with cyclic ether side groups, showing an extremely high lithium transference numbers of 0.6, but rather low lithium conductivities of  $2.8 \times 10^{-6} \text{ S cm}^{-1}$  at  $60 \text{ }^\circ\text{C}$  for poly [(1,3-dioxane-5-oxy) (1,3-dioxolane-4-methoxy)-phosphazene] [27].

Recently, we introduced the concept of polymers with immobilized anionic trifluoroborate groups. These are easy to prepare and tend to favor a good dissociation of the charge compensating lithium ions [28]. It is to be expected that the glass transition temperature will increase with the concentration of anionic substituents which, however, cannot be increased to 100% of the phosphorous sites as an increase soon will lead to much less segmental mobility of the polymer and accordingly to a slowing down of the cation mobility. The latter may be partially stopped by adding a liquid solvent to form a polymer gel. However, a compromise is an appropriate ratio of donor substituents with ether oxygens (usual lithium ion solvating groups in ether-based salt-in-polymer electrolytes) and additional more rigid anionic groups (each combined with a free lithium ion). The ratio can be optimized to achieve good ion mobility and lithium ion concentration and hence a favorable partial conductivity of lithium ions.

This work demonstrates the electrochemical properties of a mixed substituted polyphosphazene, which can be used as polymer electrolyte in combination with lithium metal anodes. The parent poly[bis(2-(2-methoxyethoxy)ethoxy)-polyphosphazene] (MEEP) with dissolved salt is already well known as a good polymer electrolyte [29–31]. The idea was to replace a moderate part of 5% to 10% of the polyether side chains at the phosphorous by fixed anionic  $-\text{OBF}_3^-$  groups which should retain the good mechanical and electrochemical properties of MEEP.

## 2. Materials and Methods

### 2.1. Starting Materials

Toluene (99.7%, VWR, Darmstadt, Germany), tetrahydrofuran (99.5%, VWR), sulfuryl chloride ( $\text{SO}_2\text{Cl}_2$ , 98%, Aldrich, Munich, Germany), *n*-pentane (98%, Baker, Gross-Gerau, Germany), phosphorous trichloride ( $\text{PCl}_3$ , 99%, Merck KGaA, Darmstadt, Germany), and 2-(2-Methoxyethoxy) ethanol ( $\text{C}_5\text{H}_{12}\text{O}_3$  99%, Aldrich) were freshly distilled beforehand. Sodium hydride (60% dispersion in mineral oil, Aldrich), sodium hydroxide (98%, Aldrich), *n*-butyl lithium solution (1.6 M in hexane, Aldrich), lithium bis(trimethylsilyl)amide ( $\text{LiN}(\text{Si}(\text{CH}_3)_3)_2$ , 97%, Aldrich), boron trifluoride diethyl etherate ( $\text{BF}_3 \cdot \text{O}(\text{C}_2\text{H}_5)_2$ , Aldrich), and phosphorous pentachloride ( $\text{PCl}_5$ , Aldrich) were kept in an argon filled glove box. The dialysis tubes ( $1.2\text{--}1.4 \times 10^{-4} \text{ g mol}^{-1}$ , Reichelt Chemietechnik, Heidelberg, Germany), Celite545<sup>®</sup> (Merck KGaA), and the molecular sieve 4 Å (VWR) used for polymer purification were cleaned and dried prior to use ( $140 \text{ }^\circ\text{C}$  for 48 h). All synthesis steps were carried out using standard vacuum line Schlenk techniques (under inert gas).

### 2.2. Synthesis of Precursor Polymer

The precursor polymer,  $[\text{NPCl}_2]_n$  (1), was synthesized based on a synthesis route published by Wang et al. [32,33] and a cationic living polymerization reaction (first published by Allcock et al. [34]) with minor modifications [35]. The intermediate poly[bis 2-(2-methoxyethoxy)ethoxy-*co*-hydroxophosphazene] (2) was obtained by nucleophilic substitution of chlorine with a corresponding ratio of sodium alcoholate and sodium hydroxide according to Figure 1. The functionalization of polyphosphazenes with oligoether side chains was already published earlier [14].

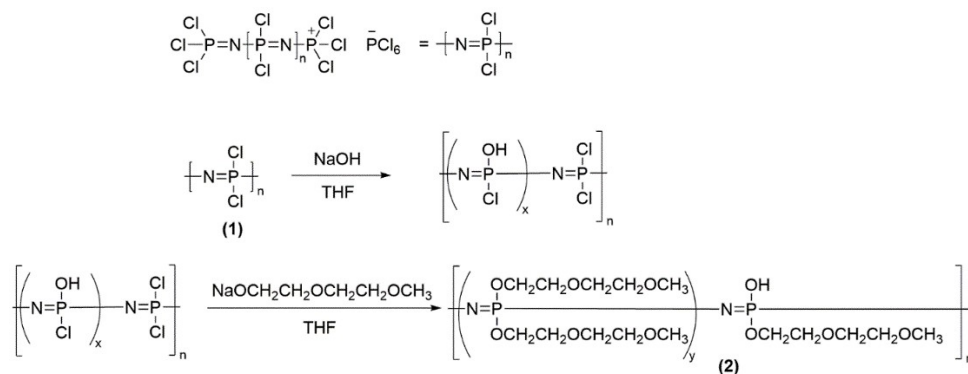


**Figure 1.** Synthesis of poly[bis 2-(2-methoxyethoxy)ethoxy-*co*-hydroxophosphazene] (2).

The final product, poly[bis 2-(2-methoxyethoxy)ethoxy-*co*-oxytrifluoroborate lithium phosphazene] (3;4), was obtained via the synthetic route described in Figure 2. The previously purified and dried poly[bis 2-(2-methoxyethoxy)ethoxy-*co*-hydroxophosphazene] (2) was dissolved in dry tetrahydrofuran and cooled to  $-40\text{ }^\circ\text{C}$  in an ice/CaCl<sub>2</sub> bath. 20 mL of 1.6 M *n*-butyl lithium (in hexane) solution was added dropwise to the polymer solution. The reaction solution was stirred for 1 h at room temperature. After the polymer was dissolved completely, the solution was cooled once again to  $40\text{ }^\circ\text{C}$  and 5 mL of boron trifluoride diethyl etherate was added dropwise afterwards. The reaction mixture was then stirred for 24 h. The final product poly[bis 2-(2-methoxyethoxy)ethoxy-*co*-oxytrifluoroborate lithium phosphazene] (3;4) with a specific substitution ratio (5 mol % in polymer 3, and 10 mol % in polymer 4) was obtained after being dried under vacuum at  $60\text{ }^\circ\text{C}$ .

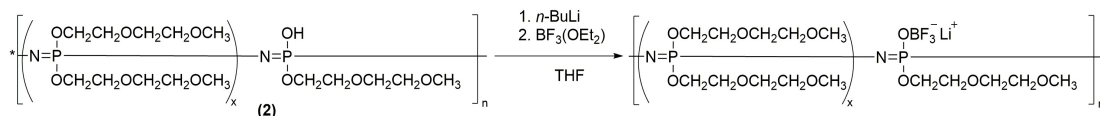


**Figure 2.** Last step of the synthesis of poly[bis 2-(2-methoxyethoxy)ethoxy-*co*-oxytrifluoroborate lithium phosphazene].

In the following, we use the abbreviations MEE-*co*-OBF<sub>3</sub>Li(5)P and MEE-*co*-OBF<sub>3</sub>Li(10)P for two series of mixed conducting polyphosphazene samples with two different concentrations 5% and 10% of the anionic oxytrifluoroborate groups referred to the total number of substituents. The oxytrifluoroborate groups were neutralized by an additional number of lithium cations.

### 2.3. Characterization of the Final Polymers

<sup>1</sup>H, <sup>11</sup>B, <sup>31</sup>P, and <sup>13</sup>C NMR spectra were acquired for examination of the product (Bruker AVANCE (III) 400 UltraShield<sup>®</sup> spectrometer, 400.03 MHz, Rheinstetten, Germany). NMR data were analyzed using Mestrelab Research S.L. MestReNova v10.0.0-14381.

The polymer was analyzed via gel permeation chromatograph (GPC) (Polymer Standards Service GmbH, Mainz, Germany) to obtain the molecular weight and distribution. The detector was calibrated in advance based on polystyrene standards (Ready-Cal standard, Polymer Standards Service GmbH, Mainz, Germany). The obtained GPC data were processed using PSS WINGPC (built 5403) software (Polymer Standards Service GmbH, SR1).

Investigation of thermal stability was done using DSC (NETZSCH DSC 204, Selb, Germany), data analysis was performed with NETZSCH software (v6.1.0). 5–10 mg of the as-synthesized polymer was sealed into an aluminum can and measured from  $-150$  to  $250\text{ }^\circ\text{C}$  with a heating rate of  $10\text{ }^\circ\text{C}/\text{min}$ . The heating cycle was repeated for another two times and the last cycle was used for interpretations.

The total ionic conductivity was measured via AC impedance spectroscopy (frequency response analyzer E 4980 A, Agilent Technologies, Waldbronn, Germany) in a frequency range from 20 Hz to 2 MHz. A peak-to-peak voltage amplitude of 40 mV was used. The polymer membranes were

sandwiched between two stainless steel electrodes (1 cm<sup>2</sup>). The measurement data were recorded in a temperature range from −20 to 90 °C, controlled by a Julabo FP45 thermostat.

Electrochemical stability windows were measured by cyclic voltammetry in three-electrode Swagelok® cells at 60 °C with a scan rate of 1 mV·s<sup>−1</sup> (Autolab PGSTAT302N, Metrohm, Filderstadt, Germany). The as-prepared salt-in-polymer membranes (thickness 200 μm) were cut into circular discs (area = 0.785 cm<sup>2</sup>). Lithium foil was employed as both the reference electrode (area = 0.393 cm<sup>2</sup>) and the counter electrode (area = 0.785 cm<sup>2</sup>). The cathodic electrode potential ranges (2.5 down to −0.5 V, against Li/Li<sup>+</sup>) were measured with a Cu working electrode (area = 0.785 cm<sup>2</sup>) while the anodic electrode potential ranges (2.5 to 7 V) were monitored with a Pt working electrode (0.785 cm<sup>2</sup>).

The lithium ion transference numbers of the as-prepared polymer electrolytes were determined via a method as described by Hiller et al. using two-electrode Swagelok® cells [36].

Impedance spectra for polymer electrolytes in symmetric cells with two lithium metal electrodes were measured using a combination of the Solartron SI 1287 potentiostat with a Solartron SI 1260 impedance analyzer in the frequency range of 1 mHz to 1 MHz with a peak-to-peak amplitude of 10 mV.

#### 2.4. Preparation of Solid Polymer Electrolyte Membranes

The as-synthesized polymers (**3,4**) were dried under vacuum at 60 °C for 1 week before use. Subsequently, around 1 g of the dried polymer was dissolved in freshly distilled THF. 10 wt % of benzophenone and 15 wt % of lithium salt were added to the solution afterwards. The solution was stirred until benzophenone and the lithium salt were dissolved completely. Then, the vessel was transferred to an oven and dried under vacuum at 60 °C for 24 h until THF was removed completely. To prepare thin membranes of the salt-in-polymer electrolyte, a suitable amount of the dried mixture was sandwiched between two Mylar®-foils and pressed to a required thickness (200–300 μm). Finally, salt-in-polymer membranes were obtained after cross-linking by applying UV-irradiation for 12 min. A series of polymer electrolyte membranes were obtained in the same way with different lithium salts (5/10 mol % -OBF<sub>3</sub>Li substituted polymers with 15 wt % LiBOB, LiTFSI, and LiFSI).

#### 2.5. Preparation of Gel Polymer Electrolyte Membranes

The as-synthesized polymers were mixed thoroughly with a calculated amount of lithium salt, ethylene carbonate–dimethyl carbonate (EC/DMC, 1:1), and benzophenone (Table S1). Subsequently, the mixture was sandwiched between two Mylar®-foils and pressed to a required thickness. The intended gel polymer electrolyte membranes (polymer **5**) were obtained after cross-linking by applying UV-irradiation for 12 min, with intermediate cooling after each minute (by dry ice). Based on our previous experience, MEEP/LiBOB gel polymer demonstrated better cyclability and possessed a more stable Li/MEEP interface as compared to gels with other lithium salts. It is evident that the bis-oxalato-borate anions support the formation of a stable and dense SEI [31,37]. Therefore, only LiBOB was used for the preparation of gel polymer electrolytes in this work.

#### 2.6. Cell Set Up

A transparent cell was combined with an optical microscope to monitor the formation and evolution of the lithium dendrites on the lithium/polymer electrolyte interface. The cell configuration is shown in Figure S1, where two narrow lithium metal strips attached to the aluminum conductor were placed on opposite areas of the composite polymer electrolyte membrane, the latter with a thickness of around ~200 μm [37]. All these assembled cell components were then put between two glass plates with a thickness of 1 mm, and further covered by PEEK to keep any gas atmosphere away from the lithium. All measurements were carried out in a dry room.

### 3. Results and Discussion

#### 3.1. Polymer Characterization

For the as-prepared polymer, an average molecular weight of  $1.5 \times 10^5$  Da and a polydispersity index (PDI) of 1.32 were determined by the GPC measurement. Two peaks appeared in the  $^{31}\text{P}$ -NMR spectra (Figure S2) of polymer (4), corresponding to di-(2-2-methoxyethoxy)ethoxy substituted phosphorous ( $-7.35$  ppm) and mono-(2-(2-methoxyethoxy)ethoxy)/mono-(lithium trifluoro borate)oxy substituted phosphorous ( $-13.53$  ppm), respectively (corresponding  $^1\text{H}$  NMR spectra shown in Figure S3). The  $\text{OBF}_3\text{-Li}$  substitution ratio is quantified to be 12%, by simply comparing the areas of integrated peaks at  $-7.35$  and  $-13.53$  ppm.  $^{19}\text{F}$ -NMR spectra of both polymer (4) and LiTFSI with a molar ratio of 1:1 are shown in Figure S4, the areas of these two observed peaks in the spectra were also used to confirm the complete reaction, indicating that the  $\text{OBF}_3\text{-Li}$  substitution ratio is around 8%. By  $^{19}\text{F}$ -NMR spectroscopy, the  $-\text{OBF}_3$  functional group was identified with a peak at  $-155.8$  ppm. These values are typical for F-atoms in  $\text{R-O-BF}_3$  species [38]. For  $^{11}\text{B}$ -NMR spectra (Figure S5), one peak was shown at  $-1.00$  ppm.

#### 3.2. Thermal Properties

Figure 3 shows the DSC heating curves of three different cross-linked polymers. It indicates that the introduction of anionic species leads to stronger ionic intermolecular interactions and decreases the segmentally movement of oligoether sidechains, since both polymer 3 and 4 exhibit higher  $T_g$  values as compared to MEEP, especially for polymer 4 with a higher substitution ratio. Nevertheless, all polymers shown here are thermally stable up to at least  $150$  °C.

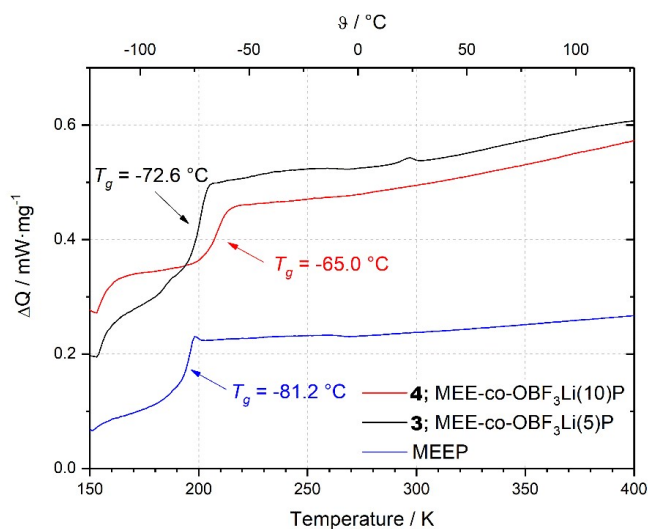


**Figure 3.** DSC Measurements of MEEP, MEE-co-OBF<sub>3</sub>Li(5)P, and MEE-co-OBF<sub>3</sub>Li(10)P.

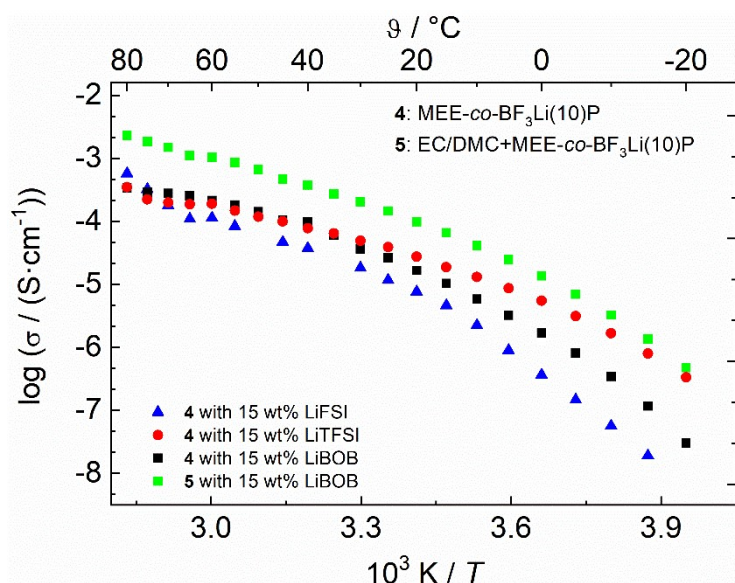
#### 3.3. Ionic Conductivity and Electrochemical Stability

Table 1 summarizes the ionic conductivities of selected polymers at certain temperatures. The ionic conductivities of the pure polymers 3 and 4 without additionally dissolved lithium salts are  $3.2 \times 10^{-6}$  and  $2.5 \times 10^{-6}$   $\text{S}\cdot\text{cm}^{-1}$ , respectively, at  $25$  °C, which are well comparable to other modified MEEP based polymers reported in the literature ( $2.5 \times 10^{-6}$   $\text{S}\cdot\text{cm}^{-1}$  as reported by Allcock;  $5 \times 10^{-9}$   $\text{S}\cdot\text{cm}^{-1}$  as reported by Fiedler, both at  $25$  °C) [26,27,39]. LiTFSI, LiFSI, and LiBOB were added to the as-prepared polymers to produce salt-in-polymer electrolyte membranes. As shown in Figure 4, polymer 4 with LiTFSI exhibits the highest ionic conductivity in the low temperature range ( $4.9 \times 10^{-5}$   $\text{S}\cdot\text{cm}^{-1}$  at  $30$  °C). While at high temperature ranges, polymer with LiFSI shows a better  $\sigma_{total}$  of  $5.0 \times 10^{-4}$   $\text{S}\cdot\text{cm}^{-1}$  at  $80$  °C.

After adding EC/DMC to the dry polymer, the total conductivity is enhanced by almost one order of magnitude. The total conductivity of polymer 5 with LiBOB reaches  $2.5 \times 10^{-3} \text{ S}\cdot\text{cm}^{-1}$  at 80 °C.

**Table 1.** Summarize of main properties of as-prepared polymers in this paper.

	$\sigma_{\text{tot}} /$ [mS·cm <sup>-1</sup> ] 25 °C	$\sigma_{\text{tot}} /$ [mS·cm <sup>-1</sup> ] 60 °C	$\sigma_{\text{Li}^+} / 10^{-3}$ [mS·cm <sup>-1</sup> ] 60 °C	T <sub>+</sub> 60 °C	T <sub>g</sub>	n(Li <sub>Salt</sub> ):n(O <sub>EO</sub> )	n(Li <sub>tot</sub> ):n(O <sub>EO</sub> )	[P=N]:O
(3)					-72.6			
MEE-co-OBF <sub>3</sub> (5)LiP								
+LiBOB	0.038	0.138	5.52	0.04	-49.7	1:26	1:21	1:5.7
+LiFSI	0.017	0.113	5.65	0.05	-49.9	1:25	1:21	1:5.7
+LiTFSI	0.037	0.171	5.13	0.03	-57.4	1:39	1:29	1:5.7
(4)					-65.0			
MEE-co-OBF <sub>3</sub> (10)LiP								
+LiBOB	0.052	0.356	17.80	0.05	-53.7	1:26	1:18	1:5.7
(5) EC/DMC+								
MEE-co-OBF <sub>3</sub> (10)LiP								
+LiBOB	0.15	1.05	220	0.18	-	1:26	1:18	1:5.7
MEEP					-81.2			
+LiBOB	0.023	0.553	22.10	0.04	-45.9	1:27	1:27	1:6

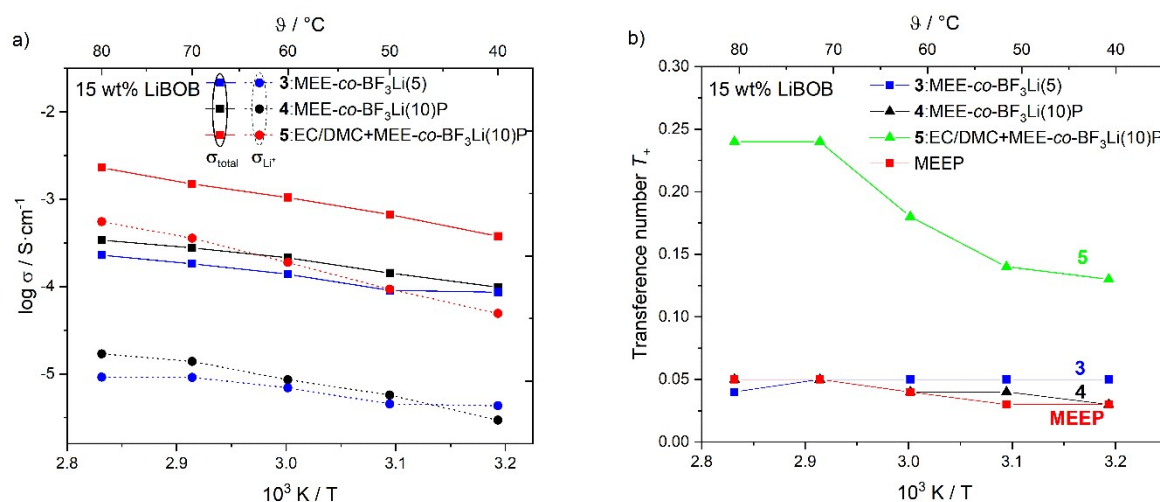


**Figure 4.** Arrhenius-plot of the cross-linked polymer 4 and 5 membranes with different lithium salts (15 wt %).

The contribution of lithium ions to the total conductivity, i.e. the partial lithium ion conductivity corresponds to the product of the total conductivity and the lithium transference number:

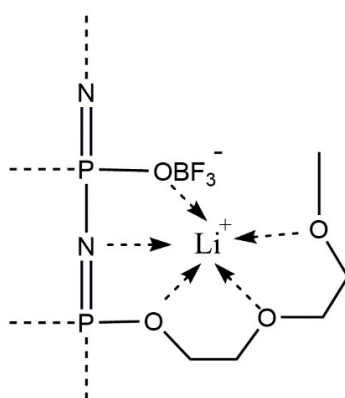
$$\sigma_{\text{Li}^+} = T_+ \cdot \sigma_{\text{total}} \tag{1}$$

Figure 5a shows the Arrhenius-type plots of the temperature dependent total conductivity,  $\sigma_{\text{total}}$ , and the partial lithium conductivity,  $\sigma_{\text{Li}^+}$ , of polymers 3,4, and 5 each containing 15 wt % dissolved LiBOB, while Figure 5b plots the corresponding lithium ion transference numbers,  $T_+$ . With a higher substitution ratio, polymer 4 shows better total and lithium conductivity compared to polymer 3 at almost all measured temperatures (except  $\sigma_{\text{Li}^+}$  at 40 °C). However, for both polymer electrolytes 3 and 4, the obtained lithium transference numbers show similar values lower than 0.1, which are lower than PEO (typically around 0.15) [15]. Desirably, the introduction of the OBF<sub>3</sub>-Li group would contribute to more mobile lithium ions, thus leading to a higher concentration of the free charge carrier and increasing lithium conductivity. However, the determined lithium transference number is only slightly better than MEEP salt-in-polymers at lower temperatures [14].



**Figure 5.** (a) Arrhenius diagram for cross-linked polymer 3, 4, and 5 with 15 wt % LiBOB showing the total and partial lithium conductivity ( $\sigma_{\text{total}}$  and  $\sigma_{\text{Li}^+}$ ). (b) Corresponding lithium transference numbers of 3, 4, 5, and MEEP.

The low lithium transference number is due to an enhanced coordination of the lithium cations by the oligoethylene oxide segments of the side chain and by the lone electron pair of the basic nitrogen atoms of the backbone [14,40]. This so-called “pocket effect” inhibits the mobility of lithium cations (see Figure 6) and could only be circumvented by a much larger concentration of  $(\text{OBF}_3)^-$  substituents along the polymer backbone. Lee et al. also discussed the strong interaction between the cations and the polymer as limiting the cation contribution to the overall conductivity [41]. Furthermore, as is demonstrated in Table 1, only a small molar increase of the total lithium ion concentration is achieved by the additional lithium counterions of the anionic groups. Therefore, further increasing the amount of substituted group or lithium salt concentration becomes necessary. Nevertheless, the salt in MEE-co-OBF<sub>3</sub>LiP membranes show good ionic conductivity at elevated temperatures  $\sim 90^\circ\text{C}$  with no indication of degradation, which indicates that such polymer electrolyte membranes have better thermal stability as compared to conventional LiPF<sub>6</sub> based organic electrolytes, especially when operating at temperatures higher than  $60^\circ\text{C}$  [42].



**Figure 6.** Illustration of coordination sites of the lithium cations by ethylene oxide sidechains, the anionic substituents and the basic nitrogen atoms in the backbone.

The addition of EC/DMC results in partial lithium ions being coordinated and transported by the carbonates in the liquid electrolyte phase [31], thus increasing the lithium transference number. The  $T_+$  value for EC/DMC+MEE-co-OBF<sub>3</sub>Li(10)P/LiBOB reaches 0.24 ( $70^\circ\text{C}$ , gel polymer), which is better than the dry salt in PEO electrolytes [15]. Hence, along with the much better total conductivity, the lithium ion conductivity of MEE-co-OBF<sub>3</sub>Li(10)P/LiBOB gel polymer is enhanced to  $3.6 \times 10^{-4} \text{ S cm}^{-1}$  at  $70^\circ\text{C}$ .

To analyze the practicability of the as-prepared polymers in combination with the lithium metal anode, lithium plating/stripping experiments for polymer 4 and 5 with different salts were performed. As is demonstrated in Figure S6, both the dry and gel polymers exhibit a relatively stable overpotential versus time profile and show no sign of severe electrolyte degradation.

Figure 7 shows the cyclic voltammogram of several anodic and cathodic cycles of polymer 4 with 15 wt % LiBOB salt at 60 °C. An anodic oxidation is evident by an increase of current density beginning at 4.5 V for the electrolyte MEE-co-OB<sub>3</sub>Li(10)P/LiBOB, which agrees with the usually reported anodic stability referred to Li<sup>+</sup>/Li for PEO based electrolytes [43,44] and is caused by irreversible oxidation within the polyether chains [14,45]. The reversible lithium plating/stripping process becomes visible in the corresponding cathodic scan (around 0 V). Maximum current densities of  $-0.80 \text{ mA}\cdot\text{cm}^{-2}$  during lithium deposition and  $0.64 \text{ mA}\cdot\text{cm}^{-2}$  during dissolution yield a coulombic efficiency of 80%. The loss of lithium indicates the formation of a SEI.

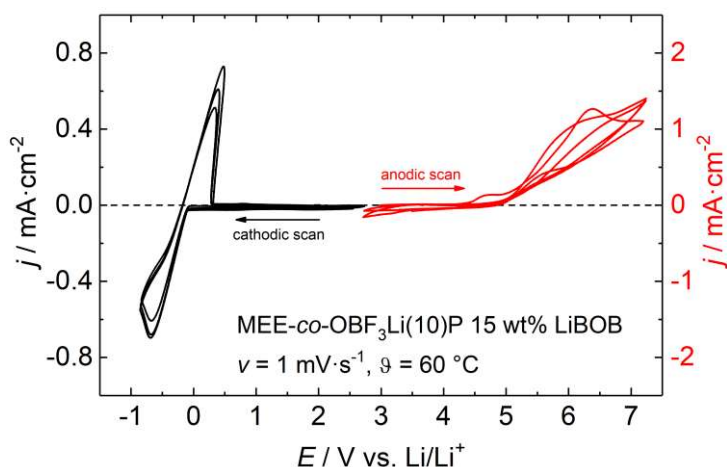


**Figure 7.** Cyclic voltammogram of MEE-co-OB<sub>3</sub>Li(10)P with 15 wt % LiBOB at 60 °C. Working electrode: Cu (for the cathodic scan on the left) and Pt (for the anodic scan on the right).

### 3.4. Analysis of Conditions for Li Dendrite Formation at the Li/MEE-co-OB<sub>3</sub>LiP (+LiBOB) Interface

To further investigate the effect of the introduced -OB<sub>3</sub>Li group on the interfacial stability, comparative studies of modified and unmodified MEEP were carried out in lithium symmetric cells with regard to reversibility and stability of lithium deposition under dc current flow. Figure 8 demonstrates the polarization curves for MEEP and MEE-co-OB<sub>3</sub>Li(10)P (both with 15 wt % LiBOB) in the visualization cell at a constant current density of  $0.1 \text{ mA}/\text{cm}^2$ . A slightly lower overpotential is observed for MEE-co-OB<sub>3</sub>Li(10)P, which suggests a lower cell impedance. A clear short-circuit is observed after a time of 65 h for the unmodified MEEP (I), corresponding to an abrupt voltage drop due to short circuit. This interpretation is confirmed by our microscope observation in Figure 9Ic, which marks the appearance of non-removable short-circuits by lithium dendrites. In addition, dendrite formation onset time ( $t_0$ ) is determined as 16 h from Figure 9Ib. Similarly, the dendrite formation onset time and short-circuit time are determined as 21 and 90 h, respectively, for MEE-co-OB<sub>3</sub>P/LiBOB; both appear to be longer as compared to MEEP/LiBOB dry polymer.

To explain this interesting difference between unmodified MEEP and BF<sub>3</sub>-modified MEEP, impedance spectra are shown in Figures 10 and 11 for MEEP and MEE-co-OB<sub>3</sub>P, respectively, each with 15 wt % LiBOB measured in the symmetric cells under open circuit potential condition.

The impedance spectra were analyzed employing ZView with the equivalent circuit displayed in Figure 10. In accordance to other polymer electrolytes in the literature [37,46,47], the high frequency intercept with the Z' axis in the left can be assigned to the polymer electrolyte bulk resistance ( $R_{el}$ ), yielding its bulk conductivity. The diameter of the large distorted semicircle can be ascribed to the interfacial resistance ( $R_{int}$ ), which can be interpreted as two partly overlapping semicircles. The latter

may be represented by a series of two different impedance contributions each consisting of a resistance element in parallel to a constant phase element. As is shown in Figure 10, these two overlapping semicircles with similar capacities can be attributed to the passivation film resistance from the solid electrolyte interface ( $R_f$ ) and the charge transfer resistance resulting from the transfer and deposition of lithium ions at the lithium metal interface ( $R_{CT}$ ). The inclined tail of the spectrum (on the low frequency end on the right) contains the impedance due to ambipolar salt diffusion during formation of concentration gradients at very small frequencies, i.e.  $\omega \rightarrow 0$ .

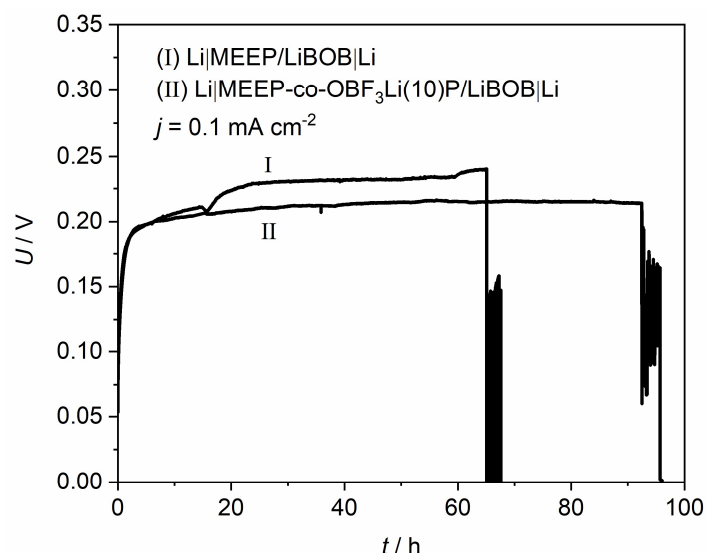


**Figure 8.** Constant current polarization curve of (I) Li|MEEP/LiBOB|Li and (II) Li|MEE-co-OBF<sub>3</sub>P/LiBOB|Li at 0.1 mA·cm<sup>-2</sup>, 60 °C.

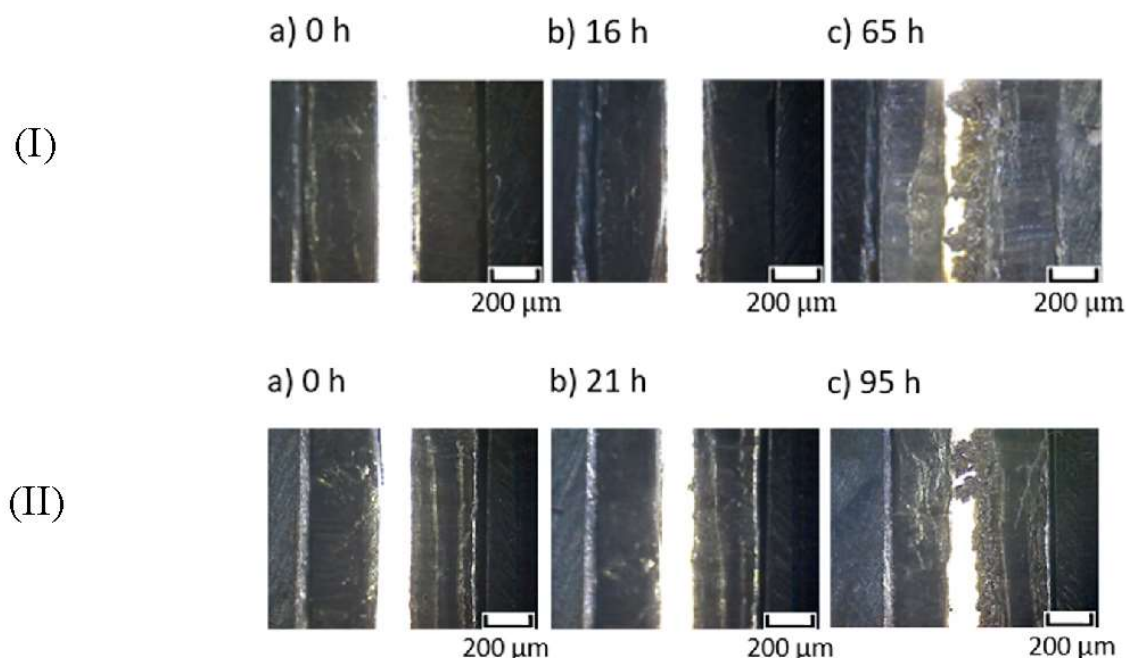


**Figure 9.** Dendrite growth in (I) Li|MEEP/LiBOB|Li and (II) Li|MEE-co-OBF<sub>3</sub>Li/LiBOB|Li visualization cell at 60 °C and 0.1 mA·cm<sup>-2</sup>; (a) before polarization; (b) dendrite structures observed; (c) dendrite reached positive electrode and short-circuit the cell.

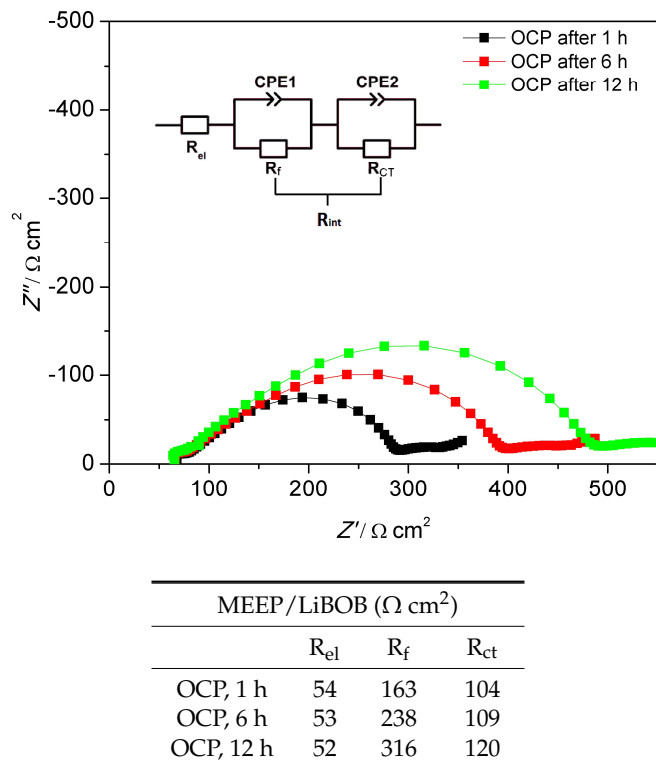


**Figure 10.** Impedance spectra of Li | MEEP/LiBOB | Li at 60 °C after 1, 6, and 12 h under OCP. The table lists the corresponding  $R_{el}$ ,  $R_f$ , and  $R_{CT}$  at different stages.  $R_{el}$  is the electrolyte bulk resistance and  $R_{int}$  is the interface resistance, which consists of  $R_f$  and  $R_{CT}$ .

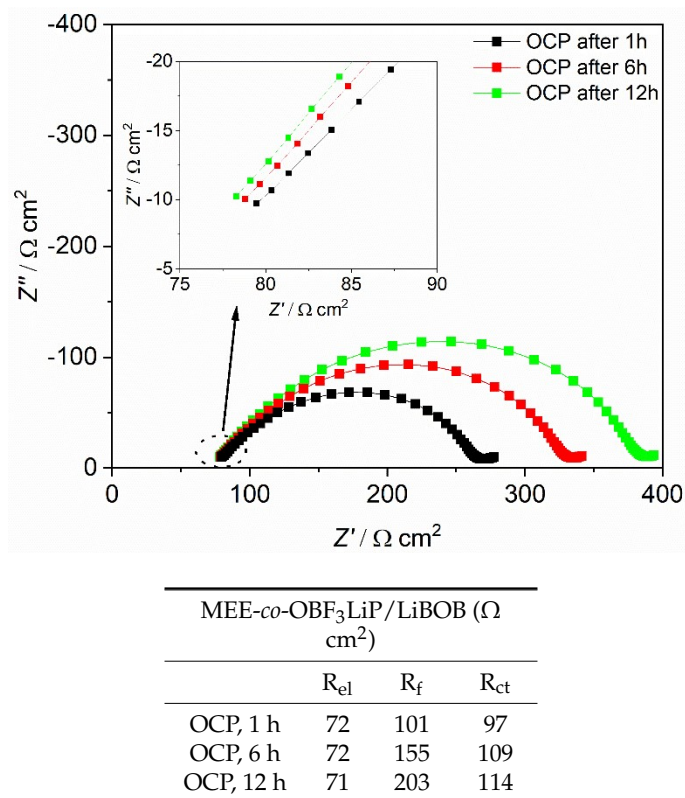


**Figure 11.** Impedance spectra of Li | MEE-co-OBF<sub>3</sub>LiP/LiBOB | Li at 60 °C after 1, 6, and 12 h under OCP conditions. The table lists the corresponding  $R_{el}$ ,  $R_f$ , and  $R_{CT}$  at different stage.  $R_{el}$  is the electrolyte bulk resistance and  $R_{int}$  is the interface resistance, which consists of  $R_f$  and  $R_{CT}$ .

For both polymer electrolytes, the bulk resistances stay almost constant during the whole resting period.  $R_{el}$  for MEEP/LiBOB is slightly lower compared to MEE-co-OBF<sub>3</sub>LiP/LiBOB, due to the slightly better total ionic conductivity of MEEP/LiBOB. On the other hand, the interface resistance dominates the cell impedance for both polymers and keeps increasing with the storage time in the measured cell, which reflects a continuous growth of the SEI at the interface, since the  $R_{CT}$  varies only slightly for both polymers. Comparison of these two figures also hints to a more conductive SEI at the Li/MEE-co-OBF<sub>3</sub>LiP interface. After 12 h of storage under the OCP condition (which is also the rest-time for cells before polarization),  $R_f$  for MEE-co-OBF<sub>3</sub>LiP/LiBOB reaches 203  $\Omega \text{ cm}^2$ , which is almost 40% lower than MEEP/LiBOB (316  $\Omega \text{ cm}^2$ ). An enhanced interfacial transport of Li<sup>+</sup> (lower  $R_{int}$ ) will postpone the time point when the cation concentration drops to zero at the anode and increase the onset time of dendrite formation according to Sand's model [37,46,48,49]. In addition, previous works in the literature have already shown that a faster lithium ion migration in the SEI (lower  $R_f$ ) would stabilize lithium electrodeposition [47,50,51]. This then gives an explanation for the better dendrite suppression effect of MEE-co-OBF<sub>3</sub>P/LiBOB as compared to MEEP/LiBOB. Moreover, the introduced -OBF<sub>3</sub> group may act as a fluoride ion source similar to the PF<sub>6</sub><sup>-</sup> anion in classic liquid lithium ion battery electrolytes as suggested by Grünebaum et al. [28]. This could result in the formation of a SEI component containing solid LiF, which was known to be able to suppress dendrite growth due to the higher surface energy and lower surface diffusion barrier for adatoms (faster diffusion along the surface) [52].

#### 4. Conclusions

In this work, we present a new type of polyphosphazene based polymer electrolyte. The introduction of boron trifluoride as the anionic species to the polyphosphazene backbone was successful. The solid polymer electrolyte membranes exhibit maximum  $\sigma_{total}$  and  $\sigma_{Li^+}$  of  $3.6 \times 10^{-4} \text{ S}\cdot\text{cm}^{-1}$  and  $1.8 \times 10^{-5} \text{ S}\cdot\text{cm}^{-1}$ , respectively, at 60 °C, which are better than the recently reported polyphosphazene based polymer electrolytes in the literature [26,27], and comparable to other salt in polymer electrolytes, like PEO:LiTFSI [36,39]. With the addition of EC/DMC, MEE-co-OBF<sub>3</sub>P gel polymer shows enhanced total and lithium conductivity, accompanied with a much higher lithium transference number ( $\sigma_{Li^+} = 0.36 \text{ mS}\cdot\text{cm}^{-1}$ ,  $T_+ = 0.24$  at 70 °C), which makes MEE-co-OBF<sub>3</sub>P gel polymer a promising electrolyte for further study.

Though a similar lithium transference number was observed as compared to MEEP/LiBOB dry polymer, MEE-co-OBF<sub>3</sub>P/LiBOB exhibits enhanced dendrite suppression ability due to the formation of more conductive SEI and the existence of F-contained SEI components (such as LiF).

Few approaches are available to further enhance the lithium conductivity of the modified MEEP, such as introducing a higher amount of substituted anion group (-OBF<sub>3</sub>Li) or lithium salts into the polymer structure to enable the lithium ion hopping mechanism, and introducing Mg<sup>2+</sup> to preferentially coordinate with ethylene oxide sidechains, which increases the amount of mobile Li<sup>+</sup> ions.

**Supplementary Materials:** The following are available online at <http://www.mdpi.com/2073-4360/10/12/1350/s1>, Figure S1, Configuration of visualization cell, reprinted from He et al. [37], Figure S2, <sup>31</sup>P NMR (376 MHz, d<sup>8</sup>-THF, 300 K) of MEE-co-OBF<sub>3</sub>LiP, (polymer 4), Figure S3, <sup>1</sup>H NMR (376 MHz, d<sup>8</sup>-THF, 300 K) of MEE-co-OBF<sub>3</sub>Li, Figure S4, <sup>19</sup>F NMR (376 MHz, d<sup>8</sup>-THF, 300 K) of MEE-co-OBF<sub>3</sub>LiP (polymer 4 with same molar LiTFSI as comparison), Figure S5, <sup>11</sup>B NMR (400 MHz, CDCl<sub>3</sub>, 300 K) of MEE-co-OBF<sub>3</sub>LiP, Figure S6, Plating/stripping experiments of (a) Li|MEE-co-OBF<sub>3</sub>LiP/LiBOB|Li (b) Li|MEE-co-OBF<sub>3</sub>LiP/ LiFSI|Li (c) Li|MEE-co-OBF<sub>3</sub>LiP/ LiTFSI|Li at 0.01 mA cm<sup>-2</sup> and (d) Li|MEE-co-OBF<sub>3</sub>LiP/LiBOB|Li, (e) gel polymer Li|EC/DMC+MEE-co-OBF<sub>3</sub>LiP/LiBOB|Li, at 0.1 mA cm<sup>-2</sup>. 15 wt % corresponding salts were used in all polymer electrolytes, Table S1, Composition of the prepared gel polymer electrolytes based on MEE-co-OBF<sub>3</sub>LiP.

**Author Contributions:** S.S. designed the synthesis route, X.H. carried out the dendrite formation study. Both authors contributed to polymer characterization and electrochemical tests, and wrote the manuscript. All authors participated in discussion and reviewed the manuscript prior to submission. S.S. and X.H. considered equal.

**Funding:** This research was funded by German federal ministry of education and research (BMBF) within the project "MEET Hi-End II" (03XP0084).

**Acknowledgments:** The authors also acknowledge the support from the graduate school of chemistry (GSC) at the University of Münster. Furthermore, the authors thank M. Hoffmeyer and C. Günther for useful hints and discussion.

**Conflicts of Interest:** The authors declare no competing interests.

## References

1. Souquet, J.L.; Duclot, M. Thin film lithium batteries. *Solid State Ion.* **2002**, *148*, 375–379. [[CrossRef](#)]
2. Belharouak, I. *Lithium Ion Batteries—New Developments*; InTech: London, UK, 2012; p. 236.
3. Patil, A.; Patil, V.; Shin, D.W.; Choi, J.-W.; Paik, D.-S.; Yoon, S.-J. Issue and challenges facing rechargeable thin film lithium batteries. *Mater. Res. Bull.* **2008**, *43*, 1913–1942. [[CrossRef](#)]
4. Hardy, L.C.; Shriver, D.F. Preparation and electrical response of solid polymer electrolytes with only one mobile species. *J. Am. Chem. Soc.* **1985**, *107*, 3823–3828. [[CrossRef](#)]
5. Jiang, Y.Y.X.; Ma, Z.; Mei, P.; Xiao, W.; You, Q.; Zhang, Y. Development of the peo based solid polymer electrolytes for all-solid state lithium ion batteries. *Polymers* **2018**, *10*, 1237. [[CrossRef](#)]
6. Zhang, H.; Li, C.; Piszcz, M.; Coya, E.; Rojo, T.; Rodriguez-Martinez, L.M.; Armand, M.; Zhou, Z. Single lithium-ion conducting solid polymer electrolytes: Advances and perspectives. *Chem. Soc. Rev.* **2017**, *46*, 797–815. [[CrossRef](#)] [[PubMed](#)]
7. Manthiram, A.; Yu, X.; Wang, S. Lithium battery chemistries enabled by solid-state electrolytes. *Nat. Rev. Mater.* **2017**, *2*, 16103. [[CrossRef](#)]
8. Song, J.Y.; Wang, Y.Y.; Wan, C.C. Review of gel-type polymer electrolytes for lithium-ion batteries. *J. Power Sources* **1999**, *77*, 183–197. [[CrossRef](#)]
9. Appetecchi, G.B.; Scaccia, S.; Passerini, S. Investigation on the stability of the lithium-polymer electrolyte interface. *J. Electrochem. Soc.* **2000**, *147*, 4448–4452. [[CrossRef](#)]
10. Ben Youcef, H.; Garcia-Calvo, O.; Lago, N.; Devaraj, S.; Armand, M. Cross-linked solid polymer electrolyte for all-solid-state rechargeable lithium batteries. *Electrochim Acta* **2016**, *220*, 587–594. [[CrossRef](#)]
11. Duan, H.; Yin, Y.-X.; Zeng, X.-X.; Li, J.-Y.; Shi, J.-L.; Shi, Y.; Wen, R.; Guo, Y.-G.; Wan, L.-J. In-situ plasticized polymer electrolyte with double-network for flexible solid-state lithium-metal batteries. *Energy Storage Mater.* **2018**, *10*, 85–91. [[CrossRef](#)]
12. Lu, Q.; He, Y.B.; Yu, Q.; Li, B.; Kaneti, Y.V.; Yao, Y.; Kang, F.; Yang, Q.H. Dendrite-free, high-rate, long-life lithium metal batteries with a 3d cross-linked network polymer electrolyte. *Adv. Mater.* **2017**, *29*, 1604460. [[CrossRef](#)] [[PubMed](#)]
13. Doyle, M.; Fuller, T.F.; Newman, J. The importance of the lithium ion transference number in lithium/polymer cells. *Electrochim. Acta* **1994**, *39*, 2073–2081. [[CrossRef](#)]
14. Jankowsky, S.; Hiller, M.M.; Wiemhöfer, H.D. Preparation and electrochemical performance of polyphosphazene based salt-in-polymer electrolyte membranes for lithium ion batteries. *J Power Sources* **2014**, *253*, 256–262. [[CrossRef](#)]
15. Edman, L.; Doeff, M.M.; Ferry, A.; Kerr, J.; De Jonghe, L.C. Transport properties of the solid polymer electrolyte system p(eo)(n)litsfi. *J. Phys. Chem. B* **2000**, *104*, 3476–3480. [[CrossRef](#)]
16. Wang, X.; Zhu, H.; Girard, G.M.; Yunis, R.; MacFarlane, D.R.; Mecerreyes, D.; Bhattacharyya, A.J.; Howlett, P.C.; Forsyth, M. Preparation and characterization of gel polymer electrolytes using poly (ionic liquids) and high lithium salt concentration ionic liquids. *J. Mater. Chem. A* **2017**, *5*, 23844–23852. [[CrossRef](#)]
17. Zuo, X.; Ma, X.; Wu, J.; Deng, X.; Xiao, X.; Liu, J.; Nan, J. Self-supporting ethyl cellulose/poly (vinylidene fluoride) blended gel polymer electrolyte for 5 v high-voltage lithium-ion batteries. *Electrochim. Acta* **2018**, *271*, 582–590. [[CrossRef](#)]
18. Shi, J.; Yang, Y.; Shao, H. Co-polymerization and blending based peo/pmma/p (vdf-hfp) gel polymer electrolyte for rechargeable lithium metal batteries. *J. Membr. Sci.* **2018**, *547*, 1–10. [[CrossRef](#)]
19. Xia, Y.; Wang, X.; Xia, X.; Xu, R.; Zhang, S.; Wu, J.; Liang, Y.; Gu, C.; Tu, J. A newly designed composite gel polymer electrolyte based on poly (vinylidene fluoride-hexafluoropropylene)(pvdf-hfp) for enhanced solid-state lithium-sulfur batteries. *Chem. A Euro. J.* **2017**, *23*, 15203–15209. [[CrossRef](#)] [[PubMed](#)]

20. Matsushita, K.; Shimazaki, Y.; Mehta, M.A.; Fujinami, T. Synthesis and characterization of aluminate polymer electrolytes and their blends with poly(ether)s. *Solid State Ion.* **2000**, *133*, 295–301. [[CrossRef](#)]
21. Fujinami, T.; Tokimune, A.; Mehta, M.A.; Shriver, D.F.; Rawsy, G.C. Siloxyaluminate polymers with high li-ion conductivity. *Chem. Mater.* **1997**, *9*, 2236–2239. [[CrossRef](#)]
22. Tada, Y.; Sato, M.; Takeno, N.; Nakacho, Y.; Shigehara, K. Attempts at lithium single-ionic conduction by anchoring sulfonate anions as terminating groups of oligo(oxyethylene) side-chains in comb-type polyphosphazenes. *Chem. Mater.* **1994**, *6*, 27–30. [[CrossRef](#)]
23. Tsuchida, E.; Kobayashi, N.; Ohno, H. Single-ion conduction in poly[(oligo(oxyethylene)methacrylate)-co-(alkali-metal methacrylates)]. *Macromolecules* **1988**, *21*, 96–100. [[CrossRef](#)]
24. Zhao, C.-Z.; Zhang, X.-Q.; Cheng, X.-B.; Zhang, R.; Xu, R.; Chen, P.-Y.; Peng, H.-J.; Huang, J.-Q.; Zhang, Q. An anion-immobilized composite electrolyte for dendrite-free lithium metal anodes. *Proc. Natl. Acad. Sci. USA* **2017**, *114*, 11069–11074. [[CrossRef](#)] [[PubMed](#)]
25. Diederichsen, K.M.; McShane, E.J.; McCloskey, B.D. Promising routes to a high li+ transference number electrolyte for lithium ion batteries. *ACS Energy Letters* **2017**, *2*, 2563–2575. [[CrossRef](#)]
26. Allcock, H.R.; Welna, D.T.; Maher, A.E. Single ion conductors–polyphosphazenes with sulfonimide functional groups. *Solid State Ion.* **2006**, *177*, 741–747. [[CrossRef](#)]
27. Fiedler, C.; Luerssen, B.; Lucht, B.; Janek, J. Synthesis and characterization of polyphosphazene electrolytes including cyclic ether side groups. *J. Power Sources* **2018**, *384*, 165–171. [[CrossRef](#)]
28. Grünebaum, M.; Buchheit, A.; Krause, D.; Hiller, M.M.; Schmidt, C.; Winter, M.; Wiemhöfer, H.-D. Development of new pyrazole-based lithium salts for battery applications – do established basic design concepts really work? *Electrochim. Acta* **2018**, *286*, 313–323. [[CrossRef](#)]
29. Kaskhedikar, N.; Paulsdorf, J.; Burjanadze, M.; Karatas, Y.; Wilmer, D.; Roling, B.; Wiemhofer, H.D. Ionic conductivity of polymer electrolyte membranes based on polyphosphazene with oligo(propylene oxide) side chains. *Solid State Ion.* **2006**, *177*, 703–707. [[CrossRef](#)]
30. Jankowsky, S.; Hiller, M.M.; Stolina, R.; Wiemhöfer, H.D. Performance of polyphosphazene based gel polymer electrolytes in combination with lithium metal anodes. *J. Power Sources* **2015**, *273*, 574–579. [[CrossRef](#)]
31. Jankowsky, S.; Hiller, M.M.; Fromm, O.; Winter, M.; Wiemhöfer, H.D. Enhanced lithium-ion transport in polyphosphazene based gel polymer electrolytes. *Electrochim. Acta* **2015**, *155*, 364–371. [[CrossRef](#)]
32. Wang, B. Development of a one-pot in situ synthesis of poly(dichlorophosphazene) from pCl<sub>3</sub>. *Macromolecules* **2005**, *38*, 643–645. [[CrossRef](#)]
33. Wang, B.; Rivard, E.; Manners, I. A new high-yield synthesis of Cl<sub>3</sub>PNSiMe<sub>3</sub>, a monomeric precursor for the controlled preparation of high molecular weight polyphosphazenes. *Inorg. Chem.* **2002**, *41*, 1690. [[CrossRef](#)] [[PubMed](#)]
34. Allcock, H.R.; Crane, C.A.; Morrissey, C.T.; Nelson, J.M.; Reeves, S.D.; Honeyman, C.H.; Manners, I. “Living” cationic polymerization of phosphoranimines as an ambient temperature route to polyphosphazenes with controlled molecular weights. *Macromolecules* **1996**, *29*, 7740–7747. [[CrossRef](#)]
35. Paulsdorf, J.; Kaskhedikar, N.; Burjanadze, M.; Obeidi, S.; Stolwijk, N.A.; Wilmer, D.; Wiemhofer, H.D. Synthesis and ionic conductivity of polymer electrolytes based on a polyphosphazene with short side groups. *Chem. Mater.* **2006**, *18*, 1281–1288. [[CrossRef](#)]
36. Hiller, M.M.; Joost, M.; Gores, H.J.; Passerini, S.; Wiemhöfer, H.D. The influence of interface polarization on the determination of lithium transference numbers of salt in polyethylene oxide electrolytes. *Electrochim. Acta* **2013**, *114*, 21–29. [[CrossRef](#)]
37. He, X.; Schmohl, S.; Wiemhöfer, H.D. Direct observation and suppression effect of lithium dendrite growth for polyphosphazene based polymer electrolytes in lithium metal cells. *ChemElectroChem.* **2018**. [[CrossRef](#)]
38. Myers, E.L.; Butts, C.P.; Aggarwal, V.K. Bf<sub>3</sub> center dot oet<sub>2</sub> and tmsotf: A synergistic combination of lewis acids. *Chem. Commun.* **2006**, 4434–4436. [[CrossRef](#)]
39. Feng, S.W.; Shi, D.Y.; Liu, F.; Zheng, L.P.; Nie, J.; Feng, W.F.; Huang, X.J.; Armand, M.; Zhou, Z.B. Single lithium-ion conducting polymer electrolytes based on poly(4-styrenesulfonyl)(trifluoromethanesulfonyl)imide anions. *Electrochim. Acta* **2013**, *93*, 254–263. [[CrossRef](#)]
40. Van Wullen, L.; Koster, T.K.J.; Wiemhofer, H.D.; Kaskhedikar, N. Local cation coordination motifs in polyphosphazene based composite electrolytes. *Chem. Mater.* **2008**, *20*, 7399–7407. [[CrossRef](#)]

41. Lee, D.K.; Allcock, H.R. The effects of cations and anions on the ionic conductivity of poly[bis(2-(2-methoxyethoxy)ethoxy)phosphazene] doped with lithium and magnesium salts of trifluoromethanesulfonate and bis(trifluoromethanesulfonyl)imide. *Solid State Ion.* **2010**, *181*, 1721–1726. [[CrossRef](#)]
42. Wilken, S.; Johansson, P.; Jacobsson, P. Infrared spectroscopy of instantaneous decomposition products of lip6-based lithium battery electrolytes. *Solid State Ion.* **2012**, *225*, 608–610. [[CrossRef](#)]
43. Kang, Y.; Lee, J.; Lee, J.-i.; Lee, C. Ionic conductivity and electrochemical properties of cross-linked solid polymer electrolyte using star-shaped siloxane acrylate. *J. Power Sources* **2007**, *165*, 92–96. [[CrossRef](#)]
44. Oh, B.; Vissers, D.; Zhang, Z.; West, R.; Tsukamoto, H.; Amine, K. New interpenetrating network type poly(siloxane-g-ethylene oxide) polymer electrolyte for lithium battery. *J. Power Sources* **2003**, *119–121*, 442–447. [[CrossRef](#)]
45. Xu, K. Nonaqueous liquid electrolytes for lithium-based rechargeable batteries. *Chem. Rev.* **2004**, *104*, 4303–4418. [[CrossRef](#)] [[PubMed](#)]
46. Liu, S.; Imanishi, N.; Zhang, T.; Hirano, A.; Takeda, Y.; Yamamoto, O.; Yang, J. Lithium dendrite formation in li/poly(ethylene oxide)–lithium bis(trifluoromethanesulfonyl)imide and n-methyl-n-propylpiperidinium bis(trifluoromethanesulfonyl)imide/li cells. *J. Electrochem. Soc.* **2010**, *157*, A1092. [[CrossRef](#)]
47. Liu, S.; Imanishi, N.; Zhang, T.; Hirano, A.; Takeda, Y.; Yamamoto, O.; Yang, J. Effect of nano-silica filler in polymer electrolyte on li dendrite formation in li/poly(ethylene oxide)–li(cf3so2)2n/li. *J. Power Sources* **2010**, *195*, 6847–6853. [[CrossRef](#)]
48. Brissot, C.; Rosso, M.; Chazalviel, J.N.; Lascaud, S. Dendritic growth mechanisms in lithium/polymer cells. *J. Power Sources* **1999**, *81–82*, 925–929. [[CrossRef](#)]
49. Brissot, C.; Rosso, M.; Chazalviel, J.N.; Baudry, P.; Lascaud, S. In situ study of dendritic growth in lithium/peo-salt/lithium cells. *Electrochim. Acta* **1998**, *43*, 1569–1574. [[CrossRef](#)]
50. Kushima, A.; So, K.P.; Su, C.; Bai, P.; Kuriyama, N.; Maebashi, T.; Fujiwara, Y.; Bazant, M.Z.; Li, J. Liquid cell transmission electron microscopy observation of lithium metal growth and dissolution: Root growth, dead lithium and lithium flotsams. *Nano Energy* **2017**, *32*, 271–279. [[CrossRef](#)]
51. Lu, Y.; Tu, Z.; Archer, L.A. Stable lithium electrodeposition in liquid and nanoporous solid electrolytes. *Nat. Mater.* **2014**, *13*, 961. [[CrossRef](#)] [[PubMed](#)]
52. Ozhaves, Y.; Gunceler, D.; Arias, T. Stability and surface diffusion at lithium-electrolyte interphases with connections to dendrite suppression. *arXiv preprint*, 2015; arXiv:1504.05799.



© 2018 by the authors. Licensee MDPI, Basel, Switzerland. This article is an open access article distributed under the terms and conditions of the Creative Commons Attribution (CC BY) license (<http://creativecommons.org/licenses/by/4.0/>).